M-MRAC for SPHERES

Vahram Stepanyan [1]
University of California Santa Cruz, Santa Cruz, CA 95064

Jonathan Barlow [2]
Stinger Ghaffarian Technologies Inc., Moffett Field, CA 94035

Jose Benavides [3]
Florida Institute for Human and Machine Cognition, Pensacola, FL 32502

Kalmanje Krishnakumar [4]
NASA Ames Research Center, Moffett Field, CA 94035

This paper presents application of the modified reference model MRAC (M-MRAC) method to control the relative position and orientation of a cluster of satellites known collectively as the Synchronized Position Hold, Engage, Reorient Experimental Satellites (SPHERES). The approach uses fast estimation algorithms to achieve guaranteed tracking of reference commands for both input and output signals in the presence of uncertainties in mass and inertia data and external disturbances. The tracking errors can be systematically decreased by the proper selection of the design parameters in the identification model. The generated control signals have acceptable magnitudes and exhibit no oscillations. The benefits of the method are demonstrated in numerical simulations.

---

[1] Senior Research Scientist, University Affiliated Research Center, NASA Ames Research Center/Mail Stop 269/3, AIAA Senior Member, email: vahram.stepanyan@nasa.gov
[2] Research Scientist, NASA Ames Research Center/Mail Stop 269/1, email: jonathan.s.barlow@nasa.gov
[3] Research Engineer, NASA Ames Research Center/Mail Stop 269/1, email: jose.v.benavides@nasa.gov
[4] Autonomous Systems and Robotics Branch Chief, Intelligent Systems Division, NASA Ames Research Center/Mail Stop 269/1, AIAA Associate Fellow, email: kalmanje.krishnakumar@nasa.gov

I. Introduction

Spacecraft relative position and attitude control problems are receiving increased attention in resent years due to their importance for autonomous proximity operations, such as International Space Station (ISS) supply and repair, automated inspection, rendezvous and docking maneuvers, and on-orbit servicing [? ?]. Accidents such as the failure of the Progress-M unmanned cargo spacecraft to autonomously rendezvous and dock with the ISS, suggest that flawless and routine implementation of autonomous proximity operations requires more fundamental research in the area of and experimentation with autonomous control systems.

There is extensive literature on control problems of spacecraft proximity operations, which include both model based and adaptive approaches. Model based approaches range from open-loop maneuver planning and ad hoc error correction [? ?], to optimal and receding horizon control [? ?], to simple linear feedback control [?], to robust control [?], to model predictive control with linear programming [?], and to model predictive control with quadratic programming and dynamically reconfigurable constraints[?], just to mention few of them. Alternatively, when the spacecraft dynamic models involve uncertainties, adaptive approaches have been used to control the relative position, see for example [? ?] and references therein.

Typically, in proximity operations linearized Hill's equations (see [?] for details) or a simple double integrator is used to describe the relative translation of the spacecraft. On the other hand, the attitude dynamics are nonlinear. Also, to avoid the singularities in the spacecraft orientation description, usually Euler parameters (sometimes called unit quaternions) are used, which also increase the order of the equations of motion. These make harder to control the spacecraft attitude. There have been lots of efforts to design controllers when the spacecraft attitude dynamics involve uncertain inertia parameters and external disturbances. Majority of these efforts use adaptive control methods to minimize the orientation or angular rate tracking errors (see for example [? ? ?] and references therein), but do not address the resulting control signal behavior. Recently, L1 adaptive control framework [1] had been introduced, which explicitly quantifies the adaptive control bounds by introducing a low-pass filter in the control channel, which a priori sets a bandwidth within which the uncertainties in the system can be compensated for.

In [2], an alternative method, called M-MRAC was introduced, which is based on the modification of the reference model by the tracking error feedback, thus preventing the system's attempt to aggressively maneuver toward the reference model in the initial stage of the process. In [3], this approach had been extended to indirect scheme, where it had also been shown that the prediction model used to estimate the system's uncertainties translates into the modified reference model by the control design. M-MRAC has a systematic design guideline and is easy to implement, yet it can guarantee desired asymptotic and transient properties for the system's input and output signals. In this paper we apply M-MRAC for the control of the small spacecraft (SPHERES) relative position and orientation in the vicinity of the International Space Station (ISS). Currently SPHERES is deployed and working onboard the ISS using simple PID controller. Although PID controllers have been sufficient in demonstrating the utility of SPHERES in controlled environments, there are few challenges that arise outside of experimental operations of SPHERES. These include: (1) modeling uncertainties; (2) environmental uncertainties while operating outside of the controlled experimental volume within the ISS; (3) operations requiring high precision positioning and pointing; (4) well behaved and predictable actuators commands; and (5) minimal control energy usage for desired maneuvers.

The rest of paper is organized as follows. In Section II we give SPHERES background information a and present the equations of motion in Section III. The control problem is formulated in Section IV. The prediction algorithm is presented in Section V, the performance of the proposed controller is analyzed in Section VI, and some concluding remarks are given in Section VIII.

II. Backgraund

The Synchronized Position Hold, Engage, Reorient Experimental Satellites (SPHERES) National Lab includes three free-flying satellites aboard the International Space Station (ISS), ground units and an air table at NASA Ames, and a SPHERES Simulator implemented in Matlab, Simulink and C code. The SPHERES satellites were originally developed by MIT, and have been used aboard the ISS since 2006. The SPHERES core software (SPHEREScore) was written with a programming interface that allows guest scientists to write code that can be executed by the SPHERES. The code

can then be loaded onto the SPHERES for on-orbit testing, and allows lower cost, lower risk testing of control algorithms and software in a microgravity environment.

Sensors. SPHERES use accelerometers, gyroscopes, and a custom global metrology system for attitude and position determination. The global metrology is a series of ultrasound transmitter beacons located at fixed, known locations. Each beacon emits an ultrasound pulse at a unique fixed delay from a timing IR pulse emitted by the primary SPHERES, and the SPHERES receive the pulses and calculate the distance to each beacon using the time of flight. The distance measurements, together with accelerometer and gyroscope measurements are used to update an extended Kalman filter [**?**].

Actuators. The only motion controlling actuators built into the SPHERES are cold-gas thrusters. Each satellite has twelve thrusters arranged in opposing pairs, with two opposing pairs per major axis of the satellite, allowing direct 6-DOF holonomic control. The thrusters are controlled by solenoids, and are either closed or fully open. The SPHEREScore software also includes a thrust mixer that converts desired forces and torques to duration of thruster firings.

Control Algorithms. The SPHEREScore software includes both state error calculation software, and position and attitude PID control software, which calculates error between a desired state and the current estimated state and generates desired forces and torques, respectively. The extended Kalman filter, thrust mixer, state error calculation software, and PID control software can each be invoked by the guest scientist software, but each can also be replaced, separately or in combination, by the guest scientist with their own software.

Simulator. The SPHERES Simulator is written in Matlab, Simulink and C, and is capable of running guest scientist code written for the SPHERES. The Simulator runs a simulated version of SPHEREScore software, and simulates communication, dynamics and other environmental interactions [**?**].

Air Table. The SPHERES National Lab has three SPHERES and an air table located at NASA Ames. The satellites and air table are available for researchers to test code and observe behavior on flight-like hardware in a 3-DOF low friction environment. This environment allows for code debugging and algorithm improvement prior to on-orbit testing, and provides software

verification and reduced risk of software malfunction. Code tested with the SPHERES on the air table can be uplinked to the ISS and loaded on the SPHERES for on-orbit testing.

III. Mathematical Model

The translational motion of SPHERES is described in relative coordinates using a coordinate frame F_s, which is attached to the ISS center of mass with x axis in the direction of the Earth's radius, y axis in the tangent direction to the ISS orbit and z axis perpendicular to the orbital plane in the direction of the ISS angular momentum. Let $\boldsymbol{r}$ be the SPHERES radius-vector in F_s

$$\boldsymbol{r} = x\boldsymbol{i} + y\boldsymbol{j} + z\boldsymbol{k}\,.$$

Assuming that ISS is on a circular orbit with a radius r_0, the SPHERES linearized relative dynamics can be represented in the Hill's form (see [**?**] for details)

$$\begin{aligned} m[\ddot{x}(t) - 3\omega_n^2 x(t) - 2\omega_n \dot{y}(t)] &= T_x(t) + d_x(t) \\ m[\ddot{y}(t) + 2\omega_n \dot{x}(t)] &= T_y(t) + d_y(t) \\ m[\ddot{z}(t) - 3\omega_n^2 z(t)] &= T_z(t) + d_z(t)\,, \end{aligned} \tag{1}$$

where m is the SPHERES mass, $\omega_n = \sqrt{\frac{\mu_G}{r_0^3}}$ is the orbital angular rate, μ_G is the gravitational constant, $\boldsymbol{T}(t) = [T_x(t)\ T_y(t)\ T_z(t)]^\top$ is the force generated by the thrusters, and $\boldsymbol{d}(t) = [d_x(t)\ d_y(t)\ d_z(t)]^\top$ is a bounded external disturbance with a bounded derivative. Equations (1) can be written in the matrix form

$$\dot{\boldsymbol{\xi}}(t) = A\boldsymbol{\xi} + \frac{1}{m} B[\boldsymbol{T}(t) + \boldsymbol{d}(t)]\,, \tag{2}$$

where we denote

$$A_n = \begin{bmatrix} 0 & 1 & 0 & 0 & 0 & 0 \\ 3\omega_n^2 & 0 & 0 & 2\omega_n & 0 & 0 \\ 0 & 0 & 0 & 1 & 0 & 0 \\ 0 & -2\omega_n & 0 & 0 & 0 & 0 \\ 0 & 0 & 0 & 0 & 1 & 0 \\ 0 & 0 & 0 & 0 & 0 & 3\omega_n^2 \end{bmatrix}, \quad B = \begin{bmatrix} 0 & 0 & 0 \\ 1 & 0 & 0 \\ 0 & 0 & 0 \\ 0 & 1 & 0 \\ 0 & 0 & 0 \\ 0 & 0 & 1 \end{bmatrix}.$$

To model the rotational motion, SPHERES is considered as a rigid body with thrusters that provide torques about three mutually perpendicular axes, which define a body-fixed coordinate frame F_b. The rotational dynamics of SPHERES are given by the equation

$$J\dot{\boldsymbol{\omega}}(t) \;=\; -\boldsymbol{\omega}(t)^{\times} J\boldsymbol{\omega}(t) + \boldsymbol{\tau}(t) + \boldsymbol{d}_r(t)\,, \tag{3}$$

where $\boldsymbol{\omega} \in \mathbb{R}^3$ is the angular velocity of the SPHERES with respect to an inertial frame F_i and expressed in the body frame F_b, $J \in \mathbb{R}^{3\times 3}$ is the inertia matrix of the SPHERES, $\boldsymbol{\tau} \in \mathbb{R}^3$ is the torque generated by the thrusters, $\boldsymbol{d}_r \in \mathbb{R}^3$ a bounded external disturbance with bounded derivative, $\boldsymbol{a}^{\times} \in \mathbb{R}^{3\times 3}$ represents the cross product operator for a vector $\boldsymbol{a} = [a_1 \; a_2 \; a_3]^{\top} \in \mathbb{R}^3$

$$\boldsymbol{a}^{\times} = \begin{bmatrix} 0 & -a_3 & a_2 \\ a_3 & 0 & -a_1 \\ -a_2 & a_1 & 0 \end{bmatrix}.$$

The orientation of the body frame F_b with respect to the inertial frame F_i is given by the Euler parameters $\boldsymbol{q} = [\boldsymbol{q}_v^{\top} \; q_4]^{\top} = [q_1 \; q_2 \; q_3 \; q_4 \;]^{\top}$, which are defined by

$$\boldsymbol{q}_v = \boldsymbol{e}\sin(\theta/2), \quad q_4 = \cos(\theta/2)\,,$$

where $\boldsymbol{e}$ is the Euler axis, and θ is the Euler angle. Euler parameters satisfy the algebraic constraint

$$\boldsymbol{q}_v^{\top}\boldsymbol{q}_v + q_4^2 = 1$$

and kinematic equations

$$\begin{aligned} \dot{\boldsymbol{q}}_v(t) &= \frac{1}{2}\left[q_4(t)\mathbb{I}_3 + \boldsymbol{q}_v(t)^{\times}\right]\boldsymbol{\omega}(t) \\ \dot{q}_4(t) &= -\frac{1}{2}\boldsymbol{q}_v^{\top}(t)\boldsymbol{\omega}(t)\,, \end{aligned} \tag{4}$$

IV. Control Problem

The translational control problem is defined as follows: design a thrusters force $\boldsymbol{T}(t)$ such that the state $\boldsymbol{\xi}(t)$ tracks the state of the reference model

$$\dot{\boldsymbol{\xi}}_m(t) = A_m\boldsymbol{\xi}_m(t) + B_m\boldsymbol{r}_{com}(t) \tag{5}$$

as close as possible assuming that m and $\boldsymbol{d}(t)$ are unknown to the controller. Here $\boldsymbol{\xi}_m \in \mathbb{R}^6$ is the state of the model, $\boldsymbol{r}_{com} \in \mathbb{R}^3$ is a piece-wise continuous and bounded external command,

$A_m = A - BK_1$ is Hurwitz, $B_m = BK_2$, and gains $K_1 \in \mathbb{R}^{3\times 6}$ and $K_2 \in \mathbb{R}^{3\times 3}$ are selected to meet the performance specifications. To this end we represent the translational dynamics in a convenient form for the identification problem

$$\dot{\boldsymbol{\xi}}(t) = A_m\boldsymbol{\xi}(t) + B_m r_{com}(t) + \frac{1}{m}B[\boldsymbol{T}(t) + m\boldsymbol{\varphi}(t) + \boldsymbol{d}(t)]\,, \tag{6}$$

where we denote $\boldsymbol{\varphi}(t) = K_1\boldsymbol{\xi}(t) + K_2\boldsymbol{r}_{com}(t)$.

Let the SPHERES desired attitude be associated with a frame F_d, the orientation of which with respect to the inertial frame F_i is given by Euler parameters $\boldsymbol{q}_d(t) = [\boldsymbol{q}_{vd}^\top(t)\ q_{4d}(t)]^\top$ satisfying the constraint $\boldsymbol{q}_{vd}^\top(t)\boldsymbol{q}_{vd}(t) + q_{4d}^2(t) = 1$. The error between the desired and current attitudes is computed according to equations

$$\begin{aligned} \boldsymbol{q}_{ve}(t) &= q_{4d}(t)\boldsymbol{q}_v(t) - q_4(t)\boldsymbol{q}_{vd}(t) + \boldsymbol{q}_v(t)^\times\boldsymbol{q}_{vd}(t) \\ q_{4e}(t) &= \boldsymbol{q}_{vd}^\top(t)\boldsymbol{q}_v(t) + q_{4d}(t)q_4(t)\,. \end{aligned} \tag{7}$$

It can be easily verified that $\boldsymbol{q}_{ve}^\top(t)\boldsymbol{q}_{ve}(t) + q_{4e}^2(t) = 1$. The corresponding rotation matrix from the body frame F_b to desired frame F_d is given by

$$C(t) = [q_{4e}^2(t) - \boldsymbol{q}_{ve}^\top(t)\boldsymbol{q}_{ve}(t)]\mathbb{I}_3 + 2\boldsymbol{q}_{ve}(t)\boldsymbol{q}_{ve}^\top(t) - 2q_{4e}(t)\boldsymbol{q}_{ve}(t)^\times\,, \tag{8}$$

and has the following properties $C^\top(t)C(t) = 1$, $\|C(t)\| = 1$, $\det(C(t)) = 1$, $\dot{C}(t) = -\boldsymbol{\omega}_e(t)^\times C(t)$, where $\boldsymbol{\omega}_e(t)$ is the angular rate error between the frames F_b and F_d. The latter is computed as

$$\boldsymbol{\omega}_e(t) = \boldsymbol{\omega}(t) - C(t)\boldsymbol{\omega}_d(t)\,, \tag{9}$$

where $\boldsymbol{\omega}_d(t)$ is the reference angular rate associated with the desired orientation $\boldsymbol{q}_d(t)$ according to equation

$$\boldsymbol{\omega}_d(t) = 2[q_{4d}(t)\dot{\boldsymbol{q}}_{vd}(t) - \dot{q}_{4d}(t)\boldsymbol{q}_{vd}(t)] - 2\boldsymbol{q}_{vd}(t)^\times\dot{\boldsymbol{q}}_{vd}(t)\,. \tag{10}$$

To derive SPHERES attitude and angular rate errors dynamics we also need the derivative of the desired angular rate, which can be expressed as

$$\dot{\boldsymbol{\omega}}_d(t) = 2[q_{4d}(t)\ddot{\boldsymbol{q}}_{vd}(t) - \ddot{q}_{4d}(t)\boldsymbol{q}_{vd}(t)] - 2\boldsymbol{q}_{vd}(t)^\times\ddot{\boldsymbol{q}}_{vd}(t)\,. \tag{11}$$

Therefore the desired attitude command $\boldsymbol{q}_d(t)$ needs to be twice differentiable.

Alternatively, we can instead use the state of a second order reference model

$$\dot{\boldsymbol{\zeta}}_1(t) = \boldsymbol{\zeta}_2(t) \tag{12}$$

$$\dot{\boldsymbol{\zeta}}_2(t) = -K_3\boldsymbol{\zeta}_2(t) - K_2[\boldsymbol{\zeta}_1(t) - \boldsymbol{q}_{vd}(t)]\,, \tag{13}$$

where $\boldsymbol{\zeta}(t) = [\boldsymbol{\zeta}_1^\top(t)\ \boldsymbol{\zeta}_2^\top(t)]^\top \in \mathbb{R}^6$ is the state of the reference model, and the gains K_3 and K_4 are chosen to make the reference model stable and to meet performance requirements. Replacing the command $\boldsymbol{q}_{vd}(t)$ with $\boldsymbol{\zeta}_1(t)$ requires to define the fourth Euler parameter command according to equation

$$q_{4d}(t) = \sqrt{1 - \boldsymbol{\zeta}_1^\top(t)\boldsymbol{\zeta}_1(t)} \tag{14}$$

for all $t \geq 0$. Clearly, one needs to specify only piecewise continuous and bounded $\boldsymbol{q}_{vd}(t)$ with this command formulation scheme. The require first and second derivatives of $\boldsymbol{q}_{vd}(t)$ are replaced with $\boldsymbol{\zeta}_2(t)$ and $-K_3\boldsymbol{\zeta}_2(t) - K_2[\boldsymbol{\zeta}_1(t) - \boldsymbol{q}_{vd}(t)]$ respectively when computing $\dot{q}_{4d}(t)$, $\ddot{q}_{4d}(t)$, $\boldsymbol{\omega}_e, \dot{\boldsymbol{\omega}}_e$.

The attitude error dynamics are given by

$$\begin{aligned} \dot{\boldsymbol{q}}_{ve}(t) &= \frac{1}{2}\left[q_{4e}(t)\mathbb{I}_3 + \boldsymbol{q}_{ve}(t)^\times\right]\boldsymbol{\omega}_e(t) \\ \dot{q}_{4e}(t) &= -\frac{1}{2}\boldsymbol{q}_{ve}^\top(t)\boldsymbol{\omega}_e(t)\,, \end{aligned} \tag{15}$$

where the angular rate error $\boldsymbol{\omega}_e(t)$ evolves according to the dynamics

$$\begin{aligned} J\dot{\boldsymbol{\omega}}_e(t) &= -[\boldsymbol{\omega}_e(t) + C(t)\boldsymbol{\omega}_d(t)]^\times J[\boldsymbol{\omega}_e(t) + C(t)\boldsymbol{\omega}_d(t)] \\ &+ J[\boldsymbol{\omega}_e(t)^\times C(t)\boldsymbol{\omega}_d(t) - C(t)\dot{\boldsymbol{\omega}}_d(t)] + \boldsymbol{\tau}(t) + \boldsymbol{d}_r(t)\,. \end{aligned} \tag{16}$$

The attitude control problem is formulated as follows: define the thrusters torque $\boldsymbol{\tau}(t)$ to regulate the error system (15)-(16) assuming that the inertia matrix J and the disturbance $\boldsymbol{d}_r(t)$ are unknown to the controller.

We notice that the angular rate dynamics (16) are much faster than the attitude kinematics (15). Therefore, time scale separation can be employed to first design a rate command $\boldsymbol{\omega}_{com}(t)$ which stabilizes the attitude error kinematics, then to design a control law for the thruster torque such that $\boldsymbol{\omega}_e(t)$ tracks the rate command $\boldsymbol{\omega}_{com}(t)$. Following [**?**] we set $\boldsymbol{\omega}_{com}(t) = -k_1\boldsymbol{\omega}_e(t)$,

where $k_1 > 0$ is a design constant. Then the attitude kinematics (15) translates to

$$\begin{aligned} \dot{\boldsymbol{q}}_{ve}(t) &= -\frac{k_1}{2} q_{4e}(t) \boldsymbol{q}_{ve}(t) \\ \dot{q}_{4e}(t) &= \frac{k_1}{2} \boldsymbol{q}_{ve}^{\top}(t) \boldsymbol{q}_{ve}(t) \,. \end{aligned} \tag{17}$$

The stability of system (17) is proved by means of the Lyapunov function candidate

$$V_0(t) = \boldsymbol{q}_{ve}^{\top}(t) \boldsymbol{q}_{ve}(t) + [q_{4e}(t) - 1]^2 \,, \tag{18}$$

the derivative of which is

$$\dot{V}_0(t) = -k_1 \boldsymbol{q}_{ve}^{\top}(t) \boldsymbol{q}_{ve}(t) \,. \tag{19}$$

Since $\dot{V}_0(t) \leq 0$, LaSalle's theorem can be applied to show that $\boldsymbol{q}_{ve}(t) \to 0$ and $q_{4e}^2(t) \to 1$ as $t \to \infty$.

Therefore, the attitude control problem is solved if we design $\boldsymbol{\tau}(t)$ such that $\boldsymbol{\omega}_e(t)$ follows $\boldsymbol{\omega}_{com}(t)$ as close as possible. To this end, we transform the dynamics (16) into a form more suitable for the parameter identification following the steps from [**?**]. Let $L : \mathbb{R}^3 \to \mathbb{R}^{3\times 6}$ be a linear operator defined for a give vector $\boldsymbol{a} = [a_1 \; a_2 \; a_3]^{\top}$ as

$$L(\boldsymbol{a}) = \begin{bmatrix} a_1 & 0 & 0 & 0 & a_3 & a_2 \\ 0 & a_2 & 0 & a_3 & 0 & a_1 \\ 0 & 0 & a_3 & a_2 & a_1 & 0 \end{bmatrix} .$$

Then the product $J\boldsymbol{a}$ can be expressed as $J\boldsymbol{a} = L(\boldsymbol{a})\boldsymbol{\theta}$, where the parameter vector $\boldsymbol{\theta} \in \mathbb{R}^6$ is associated with the inertia matrix as $\boldsymbol{\theta} = [J_{11} \; J_{22} \; J_{33} \; J_{23} \; J_{13} \; J_{12}]^{\top}$. The angular rate dynamics are written as

$$\dot{\boldsymbol{\omega}}_e(t) = \boldsymbol{g}(t) + J^{-1} \left[\Phi(t)\boldsymbol{\theta} + \boldsymbol{\tau}(t) + \boldsymbol{d}_r(t) \right] \,. \tag{20}$$

where $\boldsymbol{g}(t)$ will be specified in the control design, and

$$\Phi(t) = -\left(\boldsymbol{\omega}_e(t) + C(t)\boldsymbol{\omega}_d(t)\right)^{\times} L\left(\boldsymbol{\omega}_e(t) + C(t)\boldsymbol{\omega}_d(t)\right) + L\left(\boldsymbol{\omega}_e(t)^{\times} C(t)\boldsymbol{\omega}_d(t) - C(t)\dot{\boldsymbol{\omega}}_d(t) - \boldsymbol{g}(t)\right) \,.$$

V. Identification

First we introduce a prediction model

$$\dot{\hat{\boldsymbol{\xi}}}(t) = A_m \boldsymbol{\xi}(t) + B_m r_{com}(t) + \sigma(t) B[\boldsymbol{T}(t) + \hat{m}(t)\boldsymbol{\varphi}(t) + \hat{\boldsymbol{d}}(t)] + \lambda \tilde{\boldsymbol{\xi}}(t) \,, \tag{21}$$

for SPHERES translational dynamics, where $\hat{\boldsymbol{\xi}}(t) \in \mathbb{R}^6$ is the prediction of the translational state, $\hat{m}(t)$ is the estimate of the mass m, $\sigma(t)$ is the estimate of $\frac{1}{m}$, $\hat{\boldsymbol{d}}(t)$ is the disturbance estimate, $\tilde{\boldsymbol{\xi}}(t) = \boldsymbol{\xi}(t) - \hat{\boldsymbol{\xi}}(t)$ is the state prediction error, and $\lambda > 0$ is a design parameter. It can be noted that the prediction model reduces to

$$\dot{\hat{\boldsymbol{\xi}}}(t) = A_m \boldsymbol{\xi}(t) + B_m r_{com}(t) + \lambda \tilde{\boldsymbol{\xi}}(t)\,, \tag{22}$$

if the control force is designed according to equation

$$\boldsymbol{T}(t) = -\hat{m}(t)\boldsymbol{\varphi}(t) - \hat{\boldsymbol{d}}(t)\,, \tag{23}$$

which implies that there is no need to generate the parameter estimate $\sigma(t)$. Other estimates are generated using the adaptive laws

$$\begin{aligned} \dot{\hat{m}}(t) &= \gamma \Pr\left(\hat{m}(t),\ \tilde{\boldsymbol{\xi}}^\top(t) B \boldsymbol{\varphi}(t)\right) \\ \dot{\hat{\boldsymbol{d}}}(t) &= \gamma \Pr\left(\hat{\boldsymbol{d}}(t),\ B^\top \tilde{\boldsymbol{\xi}}(t)\right)\,, \end{aligned} \tag{24}$$

where $\gamma > 0$ is the adaptation rate and $\Pr(\cdot,\cdot)$ denotes the projection operator (see [4] for details), which is designed using the available bounds $0 < m \leq m^*$ and $|\boldsymbol{d}(t)| \leq d^*$. The prediction error satisfies the equation

$$\dot{\tilde{\boldsymbol{\xi}}}(t) = -\lambda \tilde{\boldsymbol{\xi}}(t) - \frac{1}{m} B[\tilde{m}(t)\boldsymbol{\varphi}(t) + \tilde{\boldsymbol{d}}(t)]\,, \tag{25}$$

where $\tilde{m}(t) = m - \hat{m}(t)$ and $\tilde{\boldsymbol{d}}(t) = \boldsymbol{d}(t) - \hat{\boldsymbol{d}}(t)$.

Lemma V.1 *The error signals $\tilde{\boldsymbol{\xi}}(t)$, $\tilde{m}(t)$ and $\tilde{\boldsymbol{d}}(t)$ are globally uniformly bounded, and*

$$\|\tilde{\boldsymbol{x}}(t)\| \leq \beta_2 e^{-\lambda t} + \frac{\beta_1}{\sqrt{\gamma}}\,, \tag{26}$$

where $\beta_1,\ \beta_2$ are positive constants defined in the proof.

Proof. Consider a candidate Lyapunov function

$$V(t) = \tilde{\boldsymbol{\xi}}^\top(t)\tilde{\boldsymbol{\xi}}(t) + \frac{1}{\gamma}\tilde{m}^2(t) + \frac{1}{\gamma}\tilde{\boldsymbol{d}}^\top(t)\tilde{\boldsymbol{d}}(t)\,, \tag{27}$$

the derivative of which satisfies the inequality

$$\dot{V}(t) \leq -2\lambda \boldsymbol{\xi}^\top(t)\tilde{\boldsymbol{\xi}}(t) + \frac{2}{\gamma}\tilde{\boldsymbol{d}}(t)\dot{\boldsymbol{d}}(t)\,. \tag{28}$$

Since the projection operator guarantees $|\tilde{\boldsymbol{d}}(t)| \leq 2d^*$, and $\|\dot{\boldsymbol{d}}(t)\| \leq \bar{d}^*$ for some positive constants $\bar{d}^*$, we conclude that $\dot{V}(t) \leq 0$ outside the compact set

$$\Omega = \left\{ \left(\tilde{\boldsymbol{\xi}}, \tilde{m}, \tilde{\boldsymbol{d}}\right) : \ \|\tilde{\boldsymbol{\xi}}(t)\| \leq \sqrt{\frac{4d^*\bar{d}^*}{\gamma\lambda}}, |\tilde{m}(t)| \leq 2m^*, \|\tilde{\boldsymbol{d}}(t)\| \leq d^* \right\}.$$

implying that all error signals are bounded. Using the bounds from the projection operator and the definition (27), it can be shown that $\tilde{\boldsymbol{\xi}}^\top(t)\tilde{\boldsymbol{\xi}}(t) \geq V(t) - \frac{2}{\gamma}\left[m^{*2} + d^{*2}\right]$. Therefore, the inequality (28) can be written as

$$\dot{V}(t) \leq -2\lambda \left[V(t) + \frac{1}{\gamma}\beta_1^2 \right], \tag{29}$$

where we denote $\beta_1^2 = 2m^{*2} + 2d^{*2} + \frac{4}{\lambda}d^*\bar{d}^*$. Integrating (29) we conclude that

$$V(t) \leq \left[V(0) - \frac{\beta_1^2}{\gamma} \right] e^{-2\lambda t} + \frac{\beta_1^2}{\gamma}. \tag{30}$$

Recalling that $\|\tilde{\boldsymbol{\xi}}(t)\|^2 \leq V(t)$, we obtain

$$\|\tilde{\boldsymbol{\xi}}(t)\| \leq \sqrt{\left[2V(0) - \frac{\beta_1^2}{\gamma} \right] e^{-2\lambda t} + \frac{\beta_1^2}{\gamma}}, \tag{31}$$

Taking into account that $\sqrt{a+b} \leq \sqrt{a} + \sqrt{b}$ for any $a \geq 0,\ b \geq 0$, we obtain the bound (26) with $\beta_2 = \sqrt{|2V(0) - \frac{\beta_1^2}{\gamma}|}$.

When $\boldsymbol{\xi}(t)$ and $\boldsymbol{T}(t)$ are bounded (which is provided by the control design), a tighter bound on $\tilde{\boldsymbol{\xi}}(t)$ is derived through the bounds on the adaptive signals $\boldsymbol{\eta}(t) = \tilde{m}(t)\boldsymbol{\varphi}(t) + \tilde{\boldsymbol{d}}(t)$. With this notation the prediction error dynamics take the form

$$\dot{\tilde{\boldsymbol{\xi}}}(t) = -\lambda\tilde{\boldsymbol{\xi}}(t) - \frac{1}{m}B\boldsymbol{\eta}(t), \tag{32}$$

Lemma V.2 *Let the estimates $\hat{\boldsymbol{\xi}}(t)$, $\hat{m}(t)$, and $\hat{\boldsymbol{d}}(t)$ be generated by the system (22) and (24). In addition, let $\boldsymbol{\xi}(t)$ and $\boldsymbol{T}(t)$ be bounded. Then $\boldsymbol{\eta}(t)$ and $\tilde{\boldsymbol{\xi}}(t)$ satisfy the following bounds*

$$\|\boldsymbol{\eta}(t)\| \leq \beta_3 e^{-\nu t} + \tfrac{\beta_4}{\sqrt{\gamma}} \tag{33}$$

$$\|\tilde{\boldsymbol{\xi}}(t)\| \leq \beta_5 e^{-\nu t} + \tfrac{\beta_6}{\lambda\sqrt{\gamma}}, \tag{34}$$

where the constants $\beta_i > 0,\ i = 3,4,5,6$ and $\nu > 0$ are defined in the proof.

Proof. Choosing the initial conditions of the adaptive estimates inside the regions defined by the corresponding projection operators in the adaptive laws and following [5], it is straightforward

to show that on some initial interval $[0, t_1]$, the signal $\tilde{\boldsymbol{\eta}}(t)$ satisfies the dynamics

$$\ddot{\boldsymbol{\eta}}(t) + \lambda\dot{\boldsymbol{\eta}}(t) + \tfrac{\gamma}{m}B^\top B\rho(t)\boldsymbol{\eta}(t) = -\gamma\dot{\rho}(t)\tilde{\boldsymbol{\xi}}(t) + \lambda\boldsymbol{r}_a(t) + \dot{\boldsymbol{r}}_a(t)\,, \tag{35}$$

where $\rho(t) = \boldsymbol{\varphi}^\top(t)\boldsymbol{\varphi}(t) + 1,\ \boldsymbol{r}_a(t) = \tilde{m}(t)\dot{\boldsymbol{\varphi}}(t) + \dot{\boldsymbol{d}}(t)$. Since $\boldsymbol{\xi}(t)$ and $\boldsymbol{T}(t)$ are bounded, and $\boldsymbol{\varphi}(t)$ is continuous, there exist positive constants $\delta_1,\ \delta_2,\ \delta_3$ such that $\|\rho(t)\|_{\mathcal{L}_\infty} \leq \delta_1$, $\|\dot{\rho}(t)\|_{\mathcal{L}_\infty} \leq \delta_2$ and $\|\boldsymbol{r}_a(t)\|_{\mathcal{L}_\infty} \leq \delta_3$. It follows from the results of [5] that choosing $\lambda \geq 2\sqrt{\delta_1\gamma}$ damps the oscillations in $\boldsymbol{\eta}(t)$ and guarantees the bound

$$|\boldsymbol{\eta}(t)| \leq \beta_3 e^{-\nu_1 t} + \delta_2\|\tilde{\boldsymbol{\xi}}(t)\| + \frac{\delta_4}{\sqrt{\gamma}}\|\boldsymbol{r}_a(t)\|\,, \tag{36}$$

where ν_1 is proportional to $\sqrt{\gamma}$, and the positive constants β_3 and δ_4 are independent of γ (see details in [5]). Substituting (26), we arrive at (33) with $\nu = \min(\nu_1,\ \lambda)$ and $\beta_4 = \delta_2\beta_3 + \delta_3\delta_4$.

A tighter bound on $\tilde{\boldsymbol{\xi}}(t)$ is obtained by direct integration of (32)

$$\|\tilde{\boldsymbol{\xi}}(t)\| \leq \frac{\beta_3}{m(\lambda-\nu)}\left[e^{-\nu t} - e^{-\lambda t}\right] + \frac{\beta_4}{m\lambda\sqrt{\gamma}}\left[1 - e^{-\lambda t}\right] \leq \beta_5 e^{-\nu t} + \frac{\beta_6}{\lambda\sqrt{\gamma}}\,. \tag{37}$$

The proof is complete.

Next, we introduce a prediction model for SPHERES angular rate dynamics as

$$\dot{\hat{\boldsymbol{\omega}}}_e(t) = \boldsymbol{g}(t) + \Sigma(t)\left[\Phi(t)\hat{\boldsymbol{\theta}}(t) + \boldsymbol{\tau}(t) + \hat{\boldsymbol{d}}_r(t)\right] + \lambda_r\tilde{\boldsymbol{\omega}}_e(t)\,,$$

where $\hat{\boldsymbol{\omega}}_e(t) \in \mathbb{R}^3$ is the prediction of the angular rate, $\hat{\boldsymbol{\theta}}(t)$ is the estimate of the parameter $\boldsymbol{\theta}$, $\Sigma(t)$ is the estimate of inverse of inertia matrix, $\hat{\boldsymbol{d}}_r(t)$ is the disturbance estimate, $\tilde{\boldsymbol{\omega}}(t) = \boldsymbol{\omega}(t) - \hat{\boldsymbol{\omega}}(t)$ is the angular rate prediction error, and $\lambda_r > 0$ is a design parameter. Again, it can be noticed that $\Sigma(t)$ is not required since the prediction model reduces to

$$\dot{\hat{\boldsymbol{\omega}}}_e(t) = \boldsymbol{g}(t) + \lambda_r\tilde{\boldsymbol{\omega}}_e(t)\,, \tag{38}$$

when the control torque is design as

$$\boldsymbol{\tau}(t) = -\Phi(t)\hat{\boldsymbol{\theta}}(t) - \hat{\boldsymbol{d}}_r(t)\,. \tag{39}$$

The parameter estimates are generated according to adaptive laws

$$\begin{aligned}\dot{\hat{\boldsymbol{\theta}}}(t) &= \gamma_r\,\mathrm{Pr}\left(\hat{\boldsymbol{\theta}}(t),\ \Phi^\top(t)\tilde{\boldsymbol{\omega}}(t)\right)\\ \dot{\hat{\boldsymbol{d}}}_r(t) &= \gamma_r\,\mathrm{Pr}\left(\hat{\boldsymbol{d}}_r(t),\ \tilde{\boldsymbol{\omega}}(t)\right)\,,\end{aligned} \tag{40}$$

where $\gamma_r > 0$ is the adaptation rate and the projection operator is designed using the available bounds $|\theta_i| \leq \theta_i^*,\ i = 1, \ldots, 6$ and $\|\boldsymbol{d}_r(t)\| \leq d_r^*$.

The prediction error dynamics are readily obtained to be

$$\dot{\tilde{\boldsymbol{\omega}}}_e(t) = -\lambda_r \tilde{\boldsymbol{\omega}}_e(t) - J^{-1}\left[\Phi(t)\tilde{\boldsymbol{\theta}}(t) + \tilde{\boldsymbol{d}}_r(t)\right],$$

Similar to translational dynamics, the following lemma can be proved

Lemma V.3 *Let the estimates $\hat{\boldsymbol{\omega}}_e(t)$, $\hat{\boldsymbol{\theta}}(t)$, and $\hat{\boldsymbol{d}}(t)$ be generated by the systems (38) and (40). In addition, let $\boldsymbol{\omega}(t)$ and $\boldsymbol{\tau}(t)$ be bounded. Then $\boldsymbol{\eta}_r(t) = \Phi(t)\tilde{\boldsymbol{\theta}}(t) + \tilde{\boldsymbol{d}}_r(t)$ and $\tilde{\boldsymbol{\omega}}_e(t)$ satisfy the following bounds*

$$\|\boldsymbol{\eta}_r(t)\| \leq \beta_{r3} e^{-\nu_r t} + \tfrac{\beta_{r4}}{\sqrt{\gamma_r}} \tag{41}$$

$$\|\tilde{\boldsymbol{\omega}}_e(t)\| \leq \beta_{r5} e^{-\nu_r t} + \tfrac{\beta_{r6}}{\lambda_r \sqrt{\gamma_r}}, \tag{42}$$

where the constants $\beta_{ri} > 0,\ i = 3, 4, 5, 6$ and $\nu_r > 0$ are defined similar to Lemma V.2.

VI. Controller Performance

The controller for the SPHERES translational dynamics have been already designed in the previous section according to (23). We will now show that it meets the control objective. Let $\boldsymbol{\xi}_e(t) = \boldsymbol{\xi}(t) - \boldsymbol{\xi}_m(t)$ be the tracking error. Its dynamics are derived as

$$\dot{\boldsymbol{\xi}}_e(t) = A_m \boldsymbol{\xi}_e(t) + \frac{1}{m} B[\boldsymbol{T}(t) + \hat{m}(t)\boldsymbol{\varphi}(t) + \hat{\boldsymbol{d}}(t)], \tag{43}$$

which upon substitution of the controller (23) take the form

$$\dot{\boldsymbol{\xi}}_e(t) = A_m \boldsymbol{\xi}_e(t) - \frac{1}{m} B\boldsymbol{\eta}(t). \tag{44}$$

Let $\boldsymbol{\epsilon}(t) = \boldsymbol{\xi}_e(t) - \tilde{\boldsymbol{\xi}}(t)$. It is easy to see that

$$\dot{\boldsymbol{\epsilon}}(t) = A_m \boldsymbol{\epsilon}(t) + (\lambda \mathbb{I}_6 - A_m)\tilde{\boldsymbol{\xi}}(t). \tag{45}$$

Since $\tilde{\boldsymbol{\xi}}(t)$ is bounded and A_m is stable, it follows that $\boldsymbol{\epsilon}(t)$ is bounded. Therefore, $\boldsymbol{\xi}_e(t)$ is bounded, which implies that $\boldsymbol{\xi}(t)$ is bounded, since $\boldsymbol{\xi}_m(t)$ is bounded by assumptions. Then, boundedness of $\boldsymbol{\varphi}(t)$ follows from its continuity. Hence $\boldsymbol{T}(t)$ is bounded. Therefore, Lemma V.2 can be applied.

That is the bound (33) holds. Also, for the stable matrix A_m there exist positive constants κ and ν_2 such that $\|e^{A_m t}\| \leq \kappa e^{-\nu_2 t}$. Taking into account that the reference model is much slower than the prediction model and integrating (43), we obtain similar to (37)

$$\|\boldsymbol{\xi}_e(t)\| \leq \beta_{e1} e^{-\nu_2 t} + \frac{\beta_{e2}}{\nu_2 \sqrt{\gamma}}\,. \tag{46}$$

Next, we compute a bound for the control signal (23). Let the reference control, which translates the dynamics (6) into the reference model (5) be $\boldsymbol{T}^0(t)$. Then, we obtain

$$\begin{aligned}
\|\boldsymbol{T}(t) - \boldsymbol{T}^0(t)\| &= \| - \hat{m}(t)[K_1 \xi(t) + K_2 \boldsymbol{r}_{com}(t)] - \hat{\boldsymbol{d}}(t) + m[K_1 \boldsymbol{\xi}_m(t) + K_2 \boldsymbol{r}_{com}(t)] + \boldsymbol{d}(t)\| \\
&= \|m K_1 \boldsymbol{\xi}_e(t) + \boldsymbol{\eta}(t)\| \leq m\|K_1\| \left[\beta_{e5} e^{-\nu_2 t} + \frac{\beta_{e6}}{\nu_2 \sqrt{\gamma}}\right] + \left[\beta_3 e^{-\nu t} + \frac{\beta_4}{\sqrt{\gamma}}\right] \\
&\leq \beta_{T1} e^{-\nu_2 t} + \frac{\beta_{T2}}{\sqrt{\gamma}}\,,
\end{aligned} \tag{47}$$

thus completing the proof of the following theorem.

Theorem VI.1 *Let the translational dynamics be controlled by the adaptive scheme defined via equations (22), (23), and (24). Then, all closed loop signals are bounded. The tracking error exponentially converges to a ball, the radius of which can be decreased by increasing the adaptation rate. In addition, the resulting adaptive control signal differs from the reference one by the sum of an exponentially decaying term that depends on the initialization error and a constant term, which decreases with the increase of the adaptation rate.*

Now, we design a control torque for the SPHERES using the prediction model (38). Let

$$\boldsymbol{z}(t) = \hat{\boldsymbol{\omega}}_e(t) - \boldsymbol{\omega}_{com}(t) = \hat{\boldsymbol{\omega}}_e(t) + k_1 \boldsymbol{q}_{ve}(t),$$

the dynamics of which can be easily derived as

$$\dot{\boldsymbol{z}}(t) = \boldsymbol{g}(t) + \frac{k_1}{2}\left[q_{4e}(t)\mathbb{I}_3 + \boldsymbol{q}_{ve}(t)^{\times}\right]\boldsymbol{\omega}_e(t) + \lambda_r \tilde{\boldsymbol{\omega}}_e(t).$$

Selecting

$$\boldsymbol{g}(t) = -k_2 \boldsymbol{z}(t) - \frac{k_1}{2}\left[q_{4e}(t)\mathbb{I}_3 + \boldsymbol{q}_{ve}(t)^{\times}\right]\boldsymbol{\omega}_e(t)\,, \tag{48}$$

the angular rate prediction dynamics can be written as

$$\dot{\boldsymbol{z}}(t) = -k_2 \boldsymbol{z}(t) + \lambda_r \tilde{\boldsymbol{\omega}}_e(t)\,. \tag{49}$$

Theorem VI.2 *Let SPHERES attitude be controlled by the adaptive scheme defined via equations (38), (39), (40), and (48). Then, $\boldsymbol{\omega}_e$ exponentially converges to a ball centered at $\boldsymbol{\omega}_{com}(t)$, the radius of which can be decreased by increasing the adaptation rate. In addition, the resulting adaptive control signal differs from the reference one by the sum of an exponentially decaying term that depends on the initialization error and a constant term, which decreases with the increase of the adaptation rate.*

Integrating (49) and using the bound (42) we obtain

$$\|\boldsymbol{z}(t)\| \leq \|\boldsymbol{z}(0)\|e^{-k_2 t} + \frac{\lambda_r \beta_{r5}}{(k_2 - \nu_r)}\left[e^{-\nu_r t} - e^{-k_2 t}\right] + \frac{\beta_{r6}}{k_2\sqrt{\gamma_r}}\left[1 - e^{-k_2 t}\right] \leq \beta_7 e^{-\nu_z t} + \frac{\beta_8}{\sqrt{\gamma_r}}. \quad (50)$$

where $\nu_z = \min(k_2,\ \nu_r)$, and $\beta_7,\ \beta_8$ are straightforward to compute. Since $\boldsymbol{\omega}_e(t) = \hat{\boldsymbol{\omega}}_e(t) + \tilde{\boldsymbol{\omega}}_e(t)$, it follows that

$$\|\boldsymbol{\omega}_e(t) - \boldsymbol{\omega}_{com}(t)\| = \|\boldsymbol{z}(t) + \tilde{\boldsymbol{\omega}}_e(t)\| \leq \beta_7 e^{-\nu_z t} + \frac{\beta_8}{\sqrt{\gamma_r}} + \beta_{r5} e^{-\nu_r t} + \frac{\beta_{r6}}{\lambda_r\sqrt{\gamma_r}} \leq \beta_{o1} e^{-\nu_z t} + \frac{\beta_{o2}}{\sqrt{\gamma_r}} \quad (51)$$

To compute the control torque bound, we notice that the reference controller is given by

$$\boldsymbol{\tau}^0(t) = -\Phi^0(t)\boldsymbol{\theta} - \boldsymbol{d}_r(t),$$

where

$$\Phi^0(t) = -\left(\boldsymbol{\omega}_e(t) + C(t)\boldsymbol{\omega}_d(t)\right)^{\times} L\left(\boldsymbol{\omega}_e(t) + C(t)\boldsymbol{\omega}_d(t)\right) + L\left(\boldsymbol{\omega}_e(t)^{\times} C(t)\boldsymbol{\omega}_d(t) - C(t)\dot{\boldsymbol{\omega}}_d(t) - \boldsymbol{g}^0(t)\right)$$

and $\boldsymbol{g}^0(t)$ is computed by replacing $\hat{\boldsymbol{\omega}}_e(t)$ with $\boldsymbol{\omega}_e(t)$ in (48). Therefore,

$$\Phi^0(t) - \Phi(t) = -L(\boldsymbol{g}^0(t)) + L(\boldsymbol{g}(t)) = L(\boldsymbol{g}(t) - \boldsymbol{g}^0(t)) = k_2 L(\tilde{\boldsymbol{\omega}}_e(t)).$$

It follows that

$$\begin{aligned}
\|\boldsymbol{\tau}(t) - \boldsymbol{\tau}^0(t)\| &= \|-\Phi(t)\hat{\boldsymbol{\theta}}(t) - \hat{\boldsymbol{d}}_r(t) + \Phi^0(t)\boldsymbol{\theta} + \boldsymbol{d}_r(t)\| = \|\boldsymbol{\eta}_r + [\Phi^0(t) - \Phi(t)]\boldsymbol{\theta}\| \\
&\leq \|\boldsymbol{\eta}_r(t)\| + k_2\theta^*\|L(\tilde{\boldsymbol{\omega}}_e(t))\| \quad (52) \\
&\leq \beta_{r3} e^{-\nu_r t} + \frac{\beta_{r4}}{\sqrt{\gamma_r}} + k_2\theta^*[\beta_{r5} e^{-\nu_r t} + \frac{\beta_{r6}}{\lambda_r\sqrt{\gamma_r}}] \leq \beta_{o3} e^{-\nu_r t} + \frac{\beta_{o4}}{\sqrt{\gamma_r}}. \quad (53)
\end{aligned}$$

where $\beta_{o3},\ \beta_{o4}$ are straightforward to compute. The proof is complete.

Remark VI.1 *Theorems VI.1 and VI.2 imply the input and output tracking errors can be systematically decreased by the proper choice of design parameters in the prediction/identification algorithm.*

VII. Simulation Results

We simulate the dynamics of SPHERES with $m = 4.635\ kg$ and $J = [0.0258\ 0\ 0; 0\ 0.0225\ 0; 0\ 0\ 0.023]\ kg \cdot m^2$.

The position command is $\boldsymbol{r}_{com} = [1\ 0\ 0]^\top$ meter. The reference model for the translational dynamics is chosen in the form of three decoupled second order systems of frequency $0.2236 rad/sec$ and damping ratio of 0.85. We select a disturbance that requires higher control power to counteract as compared to the control power needed for commend following. The disturbance in the translational dynamics is selected as $d_x(t) = 0.2\sin(t)$, $d_y(t)$ is a step function of magnitude 0.2 at $t = 5\ sec$ and $d_z(t)$ is a square wave of magnitude 0.15 and frequency 1 rad/sec, last two are passed trough a first order filter $\frac{10}{s+10}$ to make the derivatives bounded. The adaptive algorithm is implemented with $\gamma = 3000$ and $\lambda = 2\sqrt{\gamma}$.

The attitude command is $q_{v1d} = 0.4$, $q_{v2d} = 0.5\sin(0.5t)$, and q_{v3d} is a step function of magnitude 0.7 at $t = 10\ sec$, and q_{4d} is computed according to (14). Each component of $\boldsymbol{q}_{vd}(t)$ is filtered trough a second order stable system of frequency $0.95 rad/sec$ and damping ratio 0.85. The disturbance in the rotational dynamics is selected as $d_{rx}(t) = 0.15\sin(t)$, $d_{ry}(t)$ is a step function at $t = 15\ sec$ of magnitude 0.2 and $d_{rz}(t)$ is a square wave of magnitude 0.1 and frequency 0.8 rad/sec, last two are passed trough a first order filter $\frac{10}{s+10}$ to make the derivatives bounded.

Figure 1 displays the tracking of the translational command for 30 sec. It can be observed that good tracking performance is achieved despite the severe disturbance in all three directions. The corresponding adaptive and reference force signals are presented in Figure 2. Clearly, the control signal exhibits no oscillations and is in the acceptable magnitude range.

The attitude tracking of SPHERES is presented in Figure 3, which shows good performance in all four Euler parameters. The corresponding control torque along with the reference one is displayed in Figure 4. Once again an acceptable control signal can be observed with no oscillations.

VIII. Concluding remarks

We have presented a novel adaptive control method known as M-MRAC for SPHERES translational and rotational dynamics, which is based on fast estimation algorithms. M-MRAC guarantees

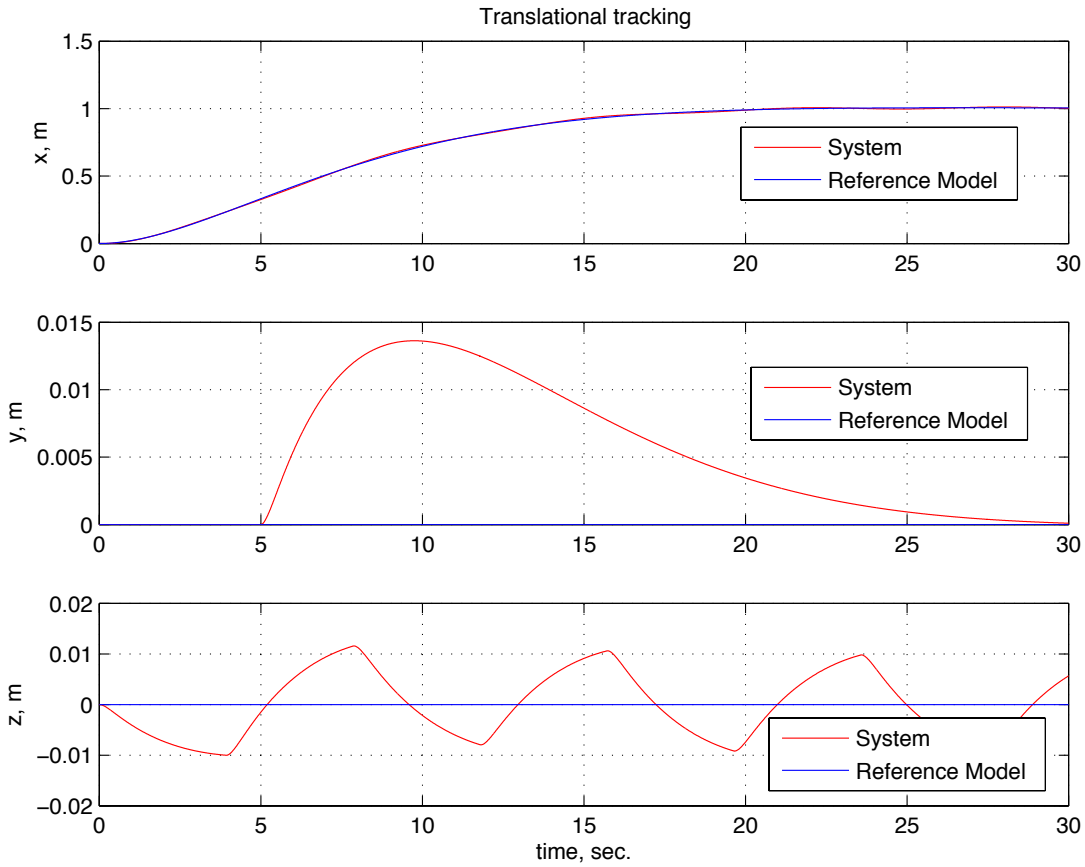

Fig. 1 Tracking of the translational command.

tracking of reference commands for both input and output signals despite the uncertainties in mass and inertia data and in the presence of external disturbances. It has been shown that the tracking errors can be systematically decreased by the proper selection of the design parameters in the identification model. The algorithm generates control signals, which have acceptable magnitudes and exhibit no oscillations, which is predicted theoretically and demonstrated in numerical simulations.

References

[1] N. Hovakimyan and C. Cao. *L1 Adaptive Control Theory.* Society for Industrial and Applied Mathematics, Philadelphia, PA, 2010.

[2] V. Stepanyan and K. Krishnakumar. MRAC Revisited: Guaranteed Performance with Reference Model Modification. *In Proc. of the American Control Conference, Baltimore, NJ*, June 2010.

[3] V. Stepanyan and K. Krishnakumar. Indirect M-MRAC for Systems with Time Varying Parameters

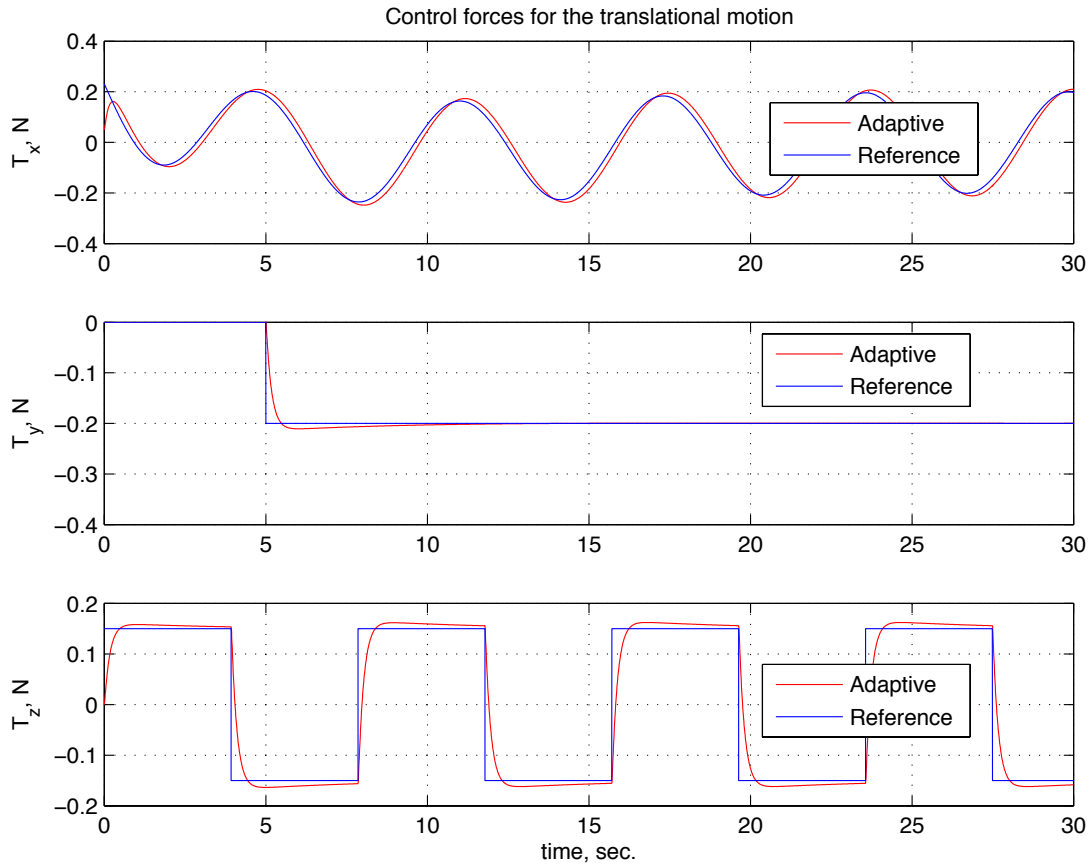

Fig. 2 Adaptive force control signal and the reference signal.

and Bounded Disturbances. *In Proc. of the IEEE Multi-Conference on Systems and Control, Dubrovnik, Croatia*, 2012.

[4] J. B. Pomet and L. Praly. Adaptive Nonlinear Regulation: Estimation from the Lyapunov Equation. *IEEE Trans. Autom. Contr.*, 37(6):729–740, 1992.

[5] V. Stepanyan and K. Krishnakumar. M-MRAC for Nonlinear Systems with Bounded Disturbances. *In Proc. of the IEEE Conference on Decision and Control, Orlando, FL*, 2011.

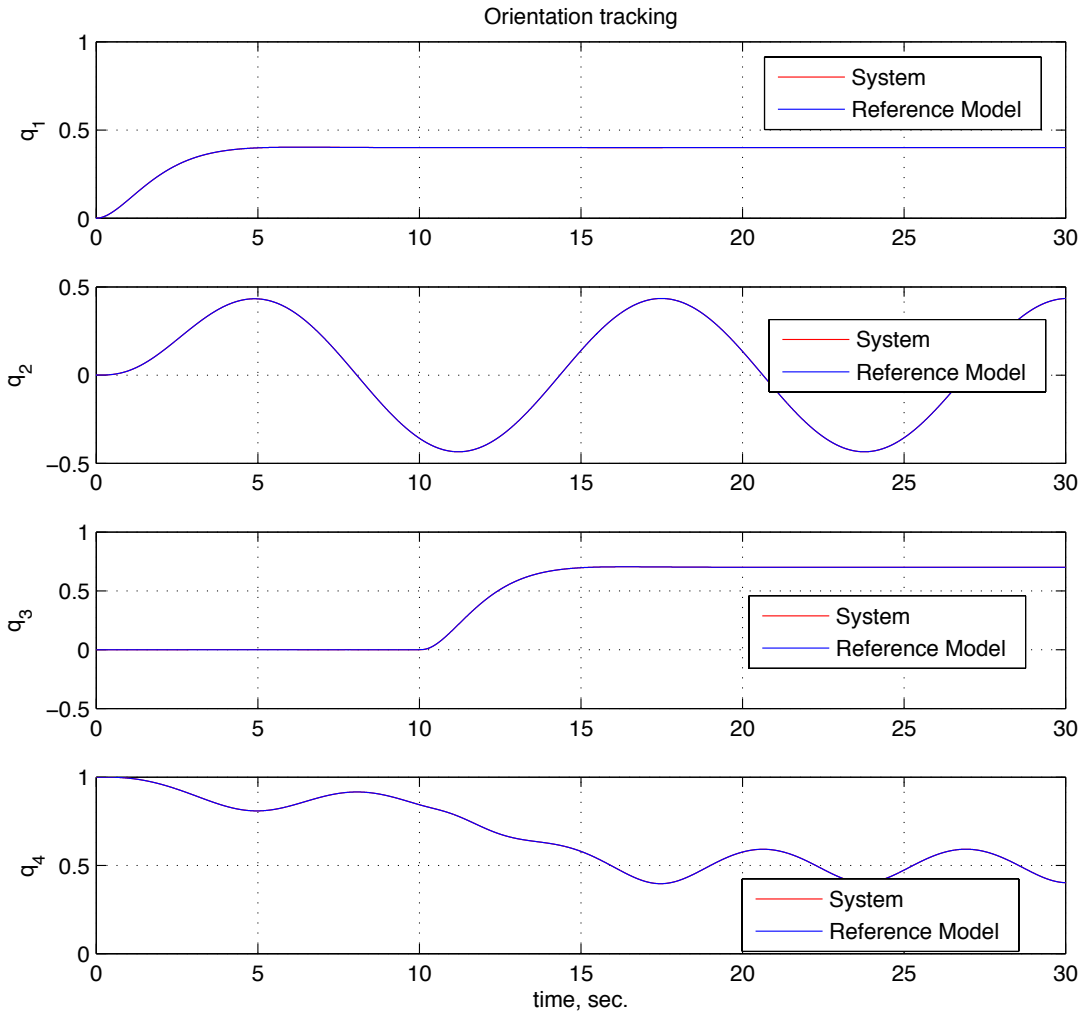

Fig. 3 Attitude command tracking.

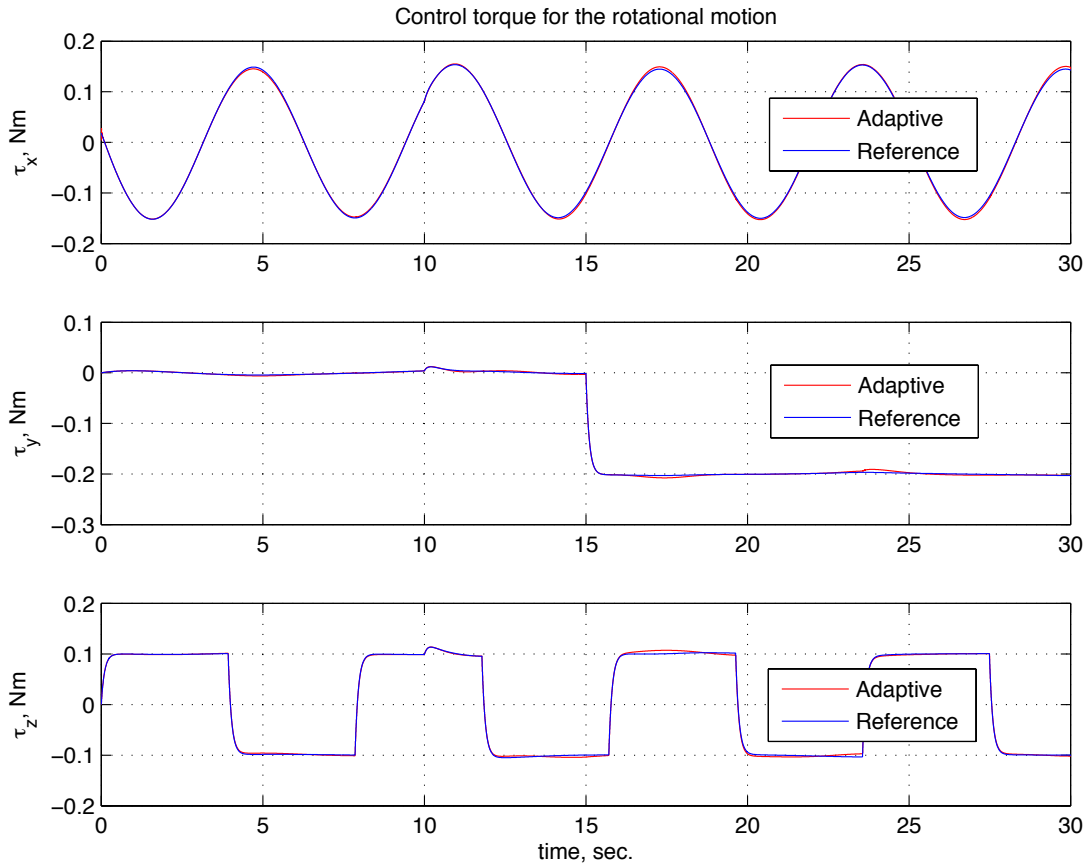

Fig. 4 Adaptive torque control signal and the reference signal.